A *cis*-element within the *ARF* locus mediates repression of *p16*^{INK4A} expression via long-range chromatin interactions

Yang Zhang[a,1], Judith Hyle[a,1], Shaela Wright[a,1], Ying Shao[b], Xujie Zhao[c], Hui Zhang[d], and Chunliang Li[a,2]

[a]Department of Tumor Cell Biology, St. Jude Children's Research Hospital, Memphis, TN 38105; [b]Department of Computational Biology, St. Jude Children's Research Hospital, Memphis, TN 38105; [c]Department of Pharmaceutical Sciences, St. Jude Children's Research Hospital, Memphis, TN 38105; and [d]Department of Hematology and Oncology, Guangzhou Women and Children's Medical Center, Guangzhou Medical University, Guangzhou, 510623 Guangdong, People's Republic of China

Loss of function of *CDKN2A/B*, also known as *INK4/ARF* [encoding p16^{INK4A}, p15^{INK4B}, and p14^{ARF} (mouse p19^{Arf})], confers susceptibility to cancers, whereas its up-regulation during organismal aging provokes cellular senescence and tissue degenerative disorders. To better understand the transcriptional regulation of *p16*^{INK4A}, a CRISPR screen targeting open, noncoding chromatin regions adjacent to *p16*^{INK4A} was performed in a human *p16*$^{INK4A-P2A-mCherry}$ reporter cell line. We identified a repressive element located in the 3′ region adjacent to the *ARF* promoter that controls *p16*^{INK4A} expression via long-distance chromatin interactions. Coinfection of lentiviral dCas9-KRAB with selected single-guide RNAs against the repressive element abrogated the *ARF/p16*^{INK4A} chromatin contacts, thus reactivating *p16*^{INK4A} expression. Genetic CRISPR screening identified candidate transcription factors inhibiting *p16*^{INK4A} regulation, including ZNF217, which was confirmed to bind the *ARF/p16*^{INK4A} interaction loop. In summary, direct physical interactions between *p16*^{INK4A} and *ARF* genes provide mechanistic insights into their cross-regulation.

chromatin conformation capture | genome editing | transcriptional regulation | knock-in | CRISPR screen

The 50-kb *CDKN2A/B* (*INK4/ARF*) locus on human chromosome 9p21 (mouse chromosome 4) is sequestered within the larger topologically associated domain (TAD) defined by the neighborhood boundary genes *MTAP* and *DMRTA1*. The *CDKN2A/B* gene cluster specifies 3 tumor suppressor proteins: p16^{INK4A}, ARF, and p15^{INK4B}. Although *p16*^{INK4A} and *ARF* messenger RNAs (mRNAs) are encoded by the common 3′ exons 2 and 3, their transcription is independently controlled by distinct promoters located 5′ to unique exon1α (*p16*^{INK4A}) and exon1β (*ARF*), which reside ∼13 kb apart. The p16^{INK4A} and p15^{INK5B} proteins are canonical cell-cycle inhibitors that bind and inactivate the cyclin-dependent kinases CDK4 and CDK6 to induce G1-phase cell-cycle arrest and contribute to cellular senescence (1–3). In contrast, ARF mainly inhibits the ubiquitin E3 ligase MDM2 to activate p53-dependent transcriptional targets. Inactivation of *ARF* and *p16*^{INK4A} in mice induces tumors with complete penetrance (4, 5), and epigenetic silencing or mutational inactivation of these genes is associated with numerous human cancers (6). Moreover, several lines of evidence suggest that naturally increased transcription of *p16*^{INK4A} and *ARF* during aging induces senescence of various cell types (7–10). Hence, understanding the regulation of these genes has major implications for cancer and age-associated degenerative disorders.

Efforts to pharmacologically restore *p16*^{INK4A} expression to suppress cancer progression have been explored through the identification of candidate small molecules and natural compounds enabling *p16*^{INK4A} reactivation (11–13), and Food and Drug Administration-approved drugs that mimic p16^{INK4A} in inhibiting CDK4 and CDK6 are now in widespread use in human

cancer treatment (3). Conversely, generalized age-dependent induction of *p16*^{INK4A} may cause deleterious effects by inducing senescence of normal tissues. Indeed, p16^{INK4A}-positive senescent cells accumulate in many tissues as animals age, and their elimination in mice tempers age-associated degenerative diseases and extends life span (14, 15).

Genome-wide association studies focusing on cancers and degenerative diseases have identified numerous single-nucleotide polymorphism (SNPs) located upstream of the *INK4/ARF* locus that fall within a superenhancer cluster of an ∼500-kb region possessing H3K27ac activity (16, 17). To investigate the function of those human aging- and cancer-associated SNPs and noncoding segments, genome editing-based screening, including clustered regularly interspaced short palindromic repeats (CRISPR) screening, provides a powerful approach (18–23). A successful CRISPR screen designed to identify functional regulatory elements of human *p16*^{INK4A} would be enhanced by a *p16*^{INK4A}-fluorescent reporter

---

Significance

Numerous human cancers exhibit silencing or inactivation of *p16*^{INK4} and *ARF*, while their increased expression is often observed in diseases of aging. The mechanism underlying the regulation of these genes is complex and not fully understood. By utilizing a human *p16*^{INK4A} reporter cell line and CRISPR libraries targeting noncoding regulatory elements and transcription factors, we discovered a *cis*-element adjacent to the *ARF* promoter that interacts with *p16*^{INK4A} via chromatin looping to mediate *p16*^{INK4A} expression. Targeting the *cis*-element or its associated transcription factors disrupts repression and induces *p16*^{INK4A} transcription. Discovery of such natural noncoding elements responsible for *p16*^{INK4A} regulation provides additional insight into the mechanism governing the dynamic regulation of this gene.

---

endogenously transcribed by the native *p16^{INK4A}* promoter in its proper chromosomal context.

There have been several efforts by other groups to derive *p16^{INK4A}* reporter cell lines. However, minimal *INK4A* promoter regulatory sequences driving a reporter did not fully mirror endogenous transcriptional regulation (24). Others engineered a large human genomic segment including the entire *INK4/ARF* gene cluster containing a firefly luciferase gene inserted into the C terminus of the *p16^{INK4A}*-coding region that was then used to generate transgenic mice (25). Similarly, Demaria et al. (26) engineered a bacterial artificial chromosome containing ∼50 kb of the murine *p16^{Ink4a}* locus, such that the *p16^{Ink4a}* promoter drove a trimodal reporter (3MR) to selectively kill senescent cells. Moreover, Baker et al. (14) generated a transgenic mouse strain by using an ∼2.6-kb fragment containing the *p16^{Ink4a}* promoter to drive the expression of a FKBP-Casp8-IRES-GFP cassette, which could conditionally eliminate senescent cells in vivo. Although all of these transgenic strains could report real-time expression of *p16^{Ink4a}* under various physical conditions or stresses, these models lack the in vivo chromatin niche that may affect more precise control of transcription when compared with that of the endogenous allele. Most recently, Liu and colleagues described a *p16^{tdTomato}* reporter allele, enabling the in vivo characterization and purification of cells featuring activation of the *p16^{Ink4a}* promoter. However, the tdTomato expression in cells depleted of a neomycin selection cassette was weakly detected and correlated less well with endogenous *p16^{Ink4a}* mRNA (27). Burd et al. (28) targeted the translational start site (TSS) of the endogenous *p16^{Ink4a}* locus by inserting the firefly luciferase complementary DNA followed by a SV40 polyadenylation signal. The resulting knock-in allele was expected to be null for *p16^{Ink4a}* expression and yet retain intronic structures surrounding exon 1β (28, 29).

Based on these considerations, we developed a *p16^{INK4A}* reporter cell line recapitulating endogenous transcriptional activity. We performed a CRISPR screen with a pooled single guide RNA (sgRNA) array targeting Assay for Transposase-Accessible Chromatin Sequencing (ATAC-seq) and H3K27ac marked regions spanning the entire TAD containing *p16^{INK4A}*, as well as a loss-of-function genetic CRISPR screen targeting 1,639 human transcription factors. We have revealed a mechanism underlying the transcriptional regulation of *p16^{INK4A}* via a *cis*-regulatory element adjacent to *ARF* promoter.

Results

Generation and Characterization of the *p16^{INK4A-P2A-mCherry}* Reporter Allele.

We utilized CRISPR/Cas9-mediated homologous recombination to deliver the *P2A-mCherry* cassette upstream of the *p16^{INK4A}* stop codon in a patient-derived human B-ALL cell line, SEM, which maintains an intact *INK4/ARF* locus (Fig. 1*A*). The *p16^{INK4A-P2A-mCherry}* reporter allele was translated in the same reading frame as p16^{INK4A}, but not ARF. Because ribosomes skip the synthesis of the glycyl-prolyl peptide bond at the C terminus of the P2A peptide, translation leads to dissociation of P2A and its immediate downstream p16^{INK4A} protein (30). Therefore, the knock-in allele produced *p16^{INK4A}* under control of the endogenous promoter and intrinsic *cis*-regulatory elements, while delivering the dissociated mCherry reporter separately.

To enable knock-in efficiency in human SEM cells, we used a double-cut nuclease cleavage strategy to release exogenous DNA fragments from a donor vector in vivo (31, 32), followed by serial sorting to enrich knock-in events (33). In brief, we constructed the knock-in vector containing a *P2A-mCherry* cassette flanked with 5′ and 3′ *p16^{INK4A}* homology arms (HAs) of ∼800 bp. The HA/knock-in cassette was bordered with a sgRNA and a protospacer adjacent motif (PAM) sequence targeting a DNA sequence 5′ of the stop codon of *p16^{INK4A}* (Dataset S1). In the presence of Cas9 and the *p16^{INK4A}* sgRNA, the HA/knock-in
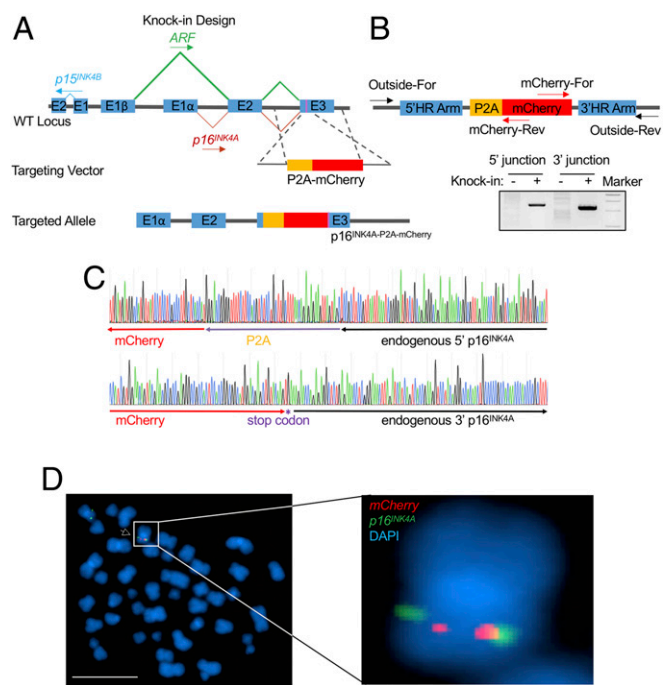

Fig. 1. Generation and characterization of the *p16^{INK4A-P2A-mCherry}* reporter allele. (*A*) Schematic diagram of the knock-in design for the *p16^{INK4A-P2A-mCherry}* reporter allele. The magenta bar in exon 3 indicates the stop codon of *p16^{INK4A}*. (*B*) Schematic diagram of the primer design for the genotyping PCR. "Outside" primers bind to endogenous loci outside the 800-bp homology arms and were used to specifically measure successful knock-in events (+) at the 5′ and 3′ boundary regions in combination with primers residing within *mCherry*. Wild-type SEM cells were used as negative controls (−). (*C*) Genotyping PCR products from the 5′ and 3′ knock-in boundaries were sequenced to verify the seamless knock-in of the *mCherry* reporter gene to the endogenous locus. (*D*) FISH of the *P2A-mCherry* knock-in cassette in *p16^{mCherry/+}* reporter cells. The *P2A-mCherry* DNA is labeled with red, and an *INK4/ARF* fosmid clone is labeled with green. Metaphase cells were scored for the correct knock-in events by pairing of red and green signals and for random integration signals. (Scale bar, 10 μm.) DAPI staining indicates the nuclei.

cassette was released from the donor vector with 2 nuclease cleavages and delivered to the target genomic region. Individual knock-in clones were derived from a targeted bulk population and characterized by genotyping PCR and Sanger sequencing (Fig. 1 *B* and *C*). A heterozygous clone carrying the *P2A-mCherry* knock-in cassette, hereafter called *p16^{mCherry/+}*, was selected for use as a reporter cell line for this study. To rule out the possibility of random integration of the reporter in the *p16^{mCherry/+}* cell line, fluorescence in situ hybridization (FISH) was performed with a *P2A-mCherry* DNA probe and a fosmid DNA probe targeting the *INK4/ARF* locus. Each of 18 metaphase cells harvested from the *p16^{mCherry/+}* cell line was identified as heterozygous for the *P2A-mCherry* knock-in cassette, yielding 2 red signals (*P2A-mCherry* probe) located adjacent to 2 of the 4 green signals (*p16^{INK4A}* probe) in each nucleus. No random integration events were observed in other chromosomes (Fig. 1*D*).

The *p16^{INK4A-P2A-Cherry}* Reporter Allele Recapitulates Endogenous Transcription of *p16^{INK4A}*.

Next, we tested whether the *p16^{INK4A-P2A-mCherry}* reporter allele would respond to the transcriptional regulation of the cellular *p16^{INK4A}* promoter. The *p16^{mCherry/+}* cells were first infected with lentivirus encoding nuclease-deficient dCas9 fused to the transcriptional repressor domain of KRAB (34) to generate a stable cell line, *p16^{mCherry/+;dCas9-KRAB}* (Fig. 2*A*). Three sgRNAs targeting the *p16^{INK4A}* promoter were cloned and delivered individually into *p16^{mCherry/+;dCas9-KRAB}* cells.
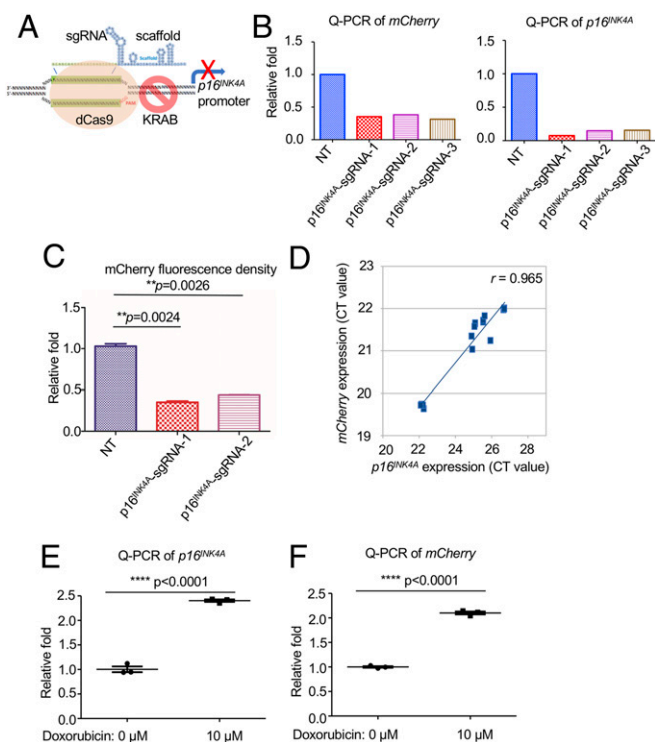
Fig. 2. The $p16^{INK4A-P2A-mCherry}$ reporter allele recapitulates endogenous transcription of $p16^{INK4A}$. (*A*) Schematic diagram of the transcriptional repression of $p16^{INK4A}$ by the CRISPR interference system. The dCas9-KRAB fusion protein was guided to the $p16^{INK4A}$ promoter with 3 individual sgRNAs. (*B*) qRT-PCR was performed on the $p16^{mCherry/+;dCas9-KRAB}$ cells with 3 different $p16^{INK4A}$-sgRNAs using primers targeting coding sequences of *mCherry* and $p16^{INK4A}$. (*C*) Flow cytometry analysis was performed on the $p16^{mCherry/+;dCas9-KRAB}$ cells with 2 $p16^{INK4A}$-sgRNAs. The mean value of the mCherry density in each group was calculated and obtained by 3 replicates. The *P* value was calculated by a 2-tailed *t* test. (*D*) The correlation of transcription reduction in *mCherry* and $p16^{INK4A}$ in response to dCas9-KRAB–mediated transcription repression (from *B*) was calculated by Pearson's correlation test ($n = 6$). (*E*) qRT-PCR was performed on the $p16^{mCherry/+}$ cells with or without the treatment of doxorubicin for 24 h by using specific primers targeting the mRNA sequence of $p16^{INK4A}$. Three biological replicates were performed. The *P* value was calculated by a 2-tailed *t* test. (*F*) qRT-PCR was performed on the $p16^{mCherry/+}$ cells with or without the treatment of doxorubicin for 24 h by using specific primers targeting the mRNA sequence of *mCherry*. Three biological replicates were performed. The *P* value was calculated by a 2-tailed *t* test.

Quantitative RT-PCR (qRT-PCR) and flow cytometry each revealed that *mCherry* and $p16^{INK4A}$ expression were suppressed by all 3 sgRNAs compared with parental $p16^{mCherry/+;dCas9-KRAB}$ cells (Fig. 2 *B* and *C*). As expected, mRNA expression of *mCherry* strongly correlated with that of $p16^{INK4A}$ when measured in cells targeted with the 3 sgRNAs and dCas9-KRAB (Pearson's $r = 0.965$) (Fig. 2*D*). In $p16^{INK4A}$-sgRNA-1–targeted cells, $p16^{INK4A}$ expression and translation were significantly reduced, resulting in elevated RB1 phosphorylation and yielding a proliferation advantage when compared with controls (*SI Appendix*, Fig. S1 *A–D*). The chemotherapy drug doxorubicin (Dox), which has been shown to activate $p16^{INK4A}$ (35), induced $p16^{INK4A}$ expression and reporter activity following 10 µM Dox treatment for 24 h (Fig. 2 *E* and *F*). Taken together, these data confirmed that the $p16^{INK4A-P2A-mCherry}$ reporter allele was expressed under the control of the endogenous promoter.

Noncoding Pooled CRISPR Screening Identified a Distal Repressive Element of $p16^{INK4A}$ Residing within the *ARF* Locus. Derivation of a reporter cell line enabled us to comprehensively conduct large-

scale screenings to identify regulatory DNA elements and proteins controlling $p16^{INK4A}$ gene expression. Since ATAC-seq measures genome-wide chromatin accessibility corresponding to genomic loci where proteins are bound to DNA, and H3K27ac marks active promoters and enhancers (36, 37), CRISPR screens against these regions could provide detailed information about *cis*-regulatory functions. Therefore, we synthesized a 2,029-sgRNA array targeting the H3K27ac and ATAC-seq positive peaks defined in human IMR90, HCT116, and SEM cells spanning the entire TAD containing the *INK4/ARF* gene cluster. Human *ARF* promoter (+1 to −4,690 bp from TSS) and $p16^{INK4A}$ promoter (+1 to −1,729 from TSS) were defined by molecular cloning and reporter assays (38). An additional 20 nontargeting (NT) sgRNAs were also included as negative controls (Fig. 3*A*). Quality control of the sgRNA library integrity by deep sequencing revealed 100% coverage of the 2,049 sgRNAs in plasmid libraries as well as HCT116 and IMR90 cells 48 h after lentiviral infection (*SI Appendix*, Fig. S2 *A–C*). Subsequently, the same lentiviral library was transduced into $p16^{mCherry/+;dCas9-KRAB}$ cells at a low multiplicity of infection (< 0.3) and then fractionated by flow cytometric sort for mCherry expression (*SI Appendix*, Fig. S3*A*). The greatest enrichment of positive control sgRNAs targeting the $p16^{INK4A}$ promoter was observed in the bottom 10% vs. top 10% mCherry sorting gate. Thereafter, the mCherry^{High} and mCherry^{Low} populations in replicate screens were selected from the top or bottom 10% sorting gates (*SI Appendix*, Fig. S3 *B* and *C*) and
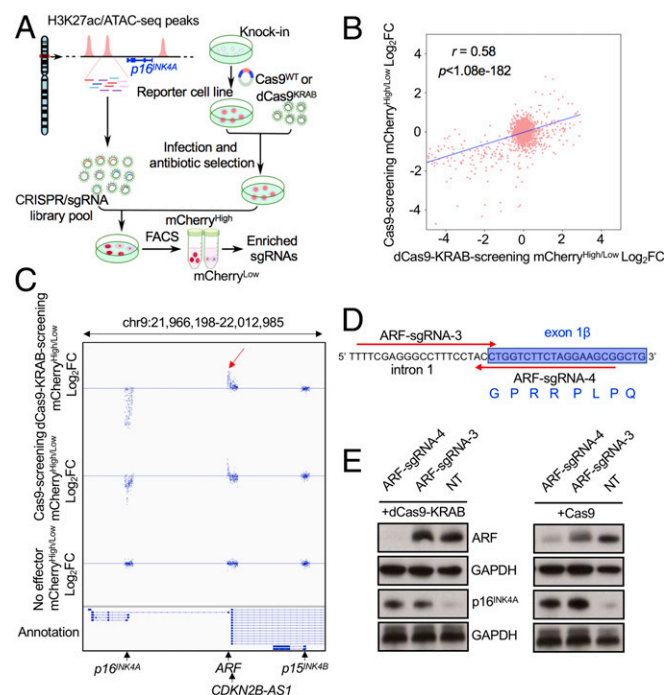

Fig. 3. Noncoding pooled CRISPR screening identified a distal repressive element of $p16^{INK4A}$ residing within the *ARF* locus. (*A*) Schematic diagram of a working model of dCas9-KRAB– and Cas9-mediated noncoding screening. (*B*) The global correlation of sgRNA distribution in dCas9-KRAB and Cas9 screens in the $p16^{mCherry/+}$ reporter cell line. (*C*) The global distribution of all sgRNAs in a selected region of the *INK4/ARF* locus from 3 screens in the $p16^{mCherry/+}$ reporter cell line using dCas9-KRAB, Cas9, and no effector control. The red arrow indicates the most enriched sgRNAs in a 42-bp region of the *ARF* exon1β and intron 1. (*D*) Two candidate sgRNAs binding to the plus and minus strands of the most enriched 42-bp core DNA sequence near the *ARF* promoter were designed for validation (ARF-sgRNA-3 and -4). The red arrows indicate the orientation of the sgRNA binding sequences. (*E*) Western blotting analysis of ARF and $p16^{INK4A}$ in dCas9-KRAB– and Cas9-expressing SEM cells infected with ARF-sgRNA-3, -4, and the nontargeting sgRNA control.

collected for deep sequencing to identify differentially represented sgRNAs, which indicated the corresponding targeted regions associated with transcriptional repression or activation of $p16^{INK4A}$, respectively. To measure the specificity of the CRISPR/dCas9-KRAB screen, we also sorted the top 10% and bottom 10% of $p16^{mCherry/+}$ parental cells transduced with the sgRNA library alone (no effector screening).

To complement the dCas9-KRAB and sgRNA library screen, we performed a parallel screen in $p16^{mCherry/+;Cas9}$ stable SEM cells (Fig. 3A). Comparisons between dCas9-KRAB and wild-type Cas9 screens demonstrated correlation of global sgRNA distribution ($r = 0.58$, $P = 1.08\text{e}{-}182$) (Fig. 3B and *SI Appendix*, Fig. S4 A and B). Data collected from 3 biological replicates were analyzed by the DESeq2 algorithm (39) for each screen. At a stringent cutoff (an adjusted P value of ≤ 0.01 and a fold-change of $\log_2^{High/Low} \geq 1$ or ≤ -1), we identified 199 differentially represented sgRNAs in the dCas9-KRAB screen (Fig. 3C and *SI Appendix*, Fig. S4 B and D). Among the 212 positive-control sgRNAs designed to target the $p16^{INK4A}$ promoter, 144 sgRNAs were significantly enriched in the mCherry^{Low} fraction. None of the 190 sgRNAs targeting the $p15^{INK4B}$ promoter were enriched. Notably, we identified 51 sgRNAs that were enriched in the mCherry^{Low} fraction, all of which targeted the *ARF* promoter and adjacent 3′ regions including exon 1β and a partial sequence of intron 1. As expected, none of the 2,049 sgRNAs were differentially represented in the no-effector screen (*SI Appendix*, Figs. S4 C and D and S5). Although the *ARF* bidirectional promoter also controls expression of the antisense long noncoding RNA *ANRIL* (also named *CDKN2B-AS1*), none of the 51 enriched sgRNAs resided on exon 1 of *ANRIL*, which is transcribed in the opposite direction. In addition, the most strongly enriched sgRNAs in the Cas9 screen recognized a minimal 42-bp DNA sequence at the junction of *ARF* exon 1β and intron 1 (Fig. 3 C and D and *SI Appendix*, Fig. S4D). Notably, this 42-bp segment includes the *ARF* exon 1β splice donor site. Therefore, combining the $p16^{INK4A}$ reporter cell line with CRISPR screening identified a previously undiscovered distal repressive regulatory region of $p16^{INK4A}$ in the *INK4/ARF* locus.

Distal Repressive Element of $p16^{INK4A}$ Composed of DNA Sequences Located 3′ and Adjacent to the *ARF* Promoter. To validate the screening results, 2 sgRNAs that resided on the 42-bp sequence between exon 1β and intron 1 (ARF-sgRNA-3 and -4) identified from the CRISPR/Cas9 screen were delivered into SEM cells stably expressing either dCas9-KRAB or Cas9 (Fig. 3 D and E). Consistent with the CRISPR/Cas9 screen in $p16^{mCherry/+}$ cells, both sgRNAs enhanced p16^{INK4A} expression through synergy with dCas9-KRAB or Cas9. In direct contrast, ARF-sgRNA-4 significantly reduced ARF expression. However, although up-regulating p16^{INK4A}, ARF-sgRNA-3 did not affect ARF expression in SEM$^{dCas9-KRAB}$ cells and only modestly suppressed ARF expression in SEM^{Cas9} cells, demonstrating that down-regulation of ARF protein expression was dispensable for p16^{INK4A} up-regulation (Fig. 3E). Two additional sgRNAs (ARF-sgRNA-1 and -2) identified in the CRISPR screen that bound to exon 1β of *ARF* and were upstream of the 42-bp core sequence also triggered some increase in $p16^{INK4A}$ expression and reporter activity (*SI Appendix*, Fig. S6 A and B). Collectively, these data suggest that the DNA sequence 3′ and adjacent to the *ARF* promoter rather than the encoded protein is a repressive element required for transcriptional regulation of $p16^{INK4A}$.

Physical Interactions between *ARF*, $p16^{INK4A}$, and $p15^{INK4B}$ Were Detected by Chromatin Conformation Capture. Given the fact that the *ARF* promoter and $p16^{INK4A}$ promoters are located ∼13 kb apart in the human genome, the transcriptional repression of $p16^{INK4A}$ by the distal repressive element might require long-distance chromatin interactions. To test this hypothesis, we deployed a multiplex assay of high-resolution chromatin con-

formation called Capture-C (40, 41), a derivative of the chromatin conformation capture (3C) technique coupled with oligonucleotide enrichment and high-throughput sequencing. This method enables the discovery of distant interacting elements from multiple "bait" sites (or anchor regions) with high resolution. Here, Capture-C was performed using a 3C library prepared from SEM cells. Two biotinylated bait oligonucleotides were designed to hybridize to each of the H3K27ac peaks overlapping the defined $p16^{INK4A}$, *ARF*, and $p15^{INK4B}$ promoters, respectively. Strong enrichment of sequences at each bait site confirmed the efficiency of hybridization. Using baits against the $p16^{INK4A}$ promoter, a broad peak encompassing part of the *ARF* promoter including the identified distal repressive element affecting $p16^{INK4A}$ was identified as a strong interacting region. Similarly, when bait oligonucleotides were hybridized with the $p15^{INK4B}$ promoter, a strong interaction between $p15^{INK4B}$ and *ARF* was observed. When Capture-C was carried out using the *ARF* promoter oligonucleotides as bait, both $p16^{INK4A}$ and $p15^{INK4B}$ were captured. These data suggest that in SEM cells the *ARF* locus physically interacts with both $p16^{INK4A}$ and $p15^{INK4B}$ through long-distance chromatin looping (Fig. 4A). However, since direct contact between $p16^{INK4A}$ and $p15^{INK4B}$ was not observed, we reasoned that *ARF*/$p16^{INK4A}$ and *ARF*/$p15^{INK4B}$ associate in separate looping complexes.

To independently confirm the physical interaction between *ARF* and $p16^{INK4A}$, we deployed a recently developed CUT&RUN strategy (42) in which antibody-targeted controlled cleavage by micrococcal nuclease releases specific protein-DNA complexes into the supernatant for paired-end DNA sequencing. Because CUT&RUN is performed in situ, it enables both quantitative high-resolution chromatin mapping of a local chromatin environment and identification of physical DNA interactions. Here, we performed CUT&RUN in SEM cells stably expressing dCas9-KRAB and sgRNAs targeting the $p16^{INK4A}$ repressive element (ARF-sgRNA-1 and -2). By using a Cas9 antibody that recognizes dCas9 for pull-down, we clearly detected dCas9-binding peaks in the sgRNA-guided sequences in the *ARF* and $p16^{INK4A}$ loci simultaneously, demonstrating that these regions were physically interacting in situ. Similarly, in SEM$^{dCas9-KRAB}$ cells transduced with sgRNAs targeting the $p16^{INK4A}$ promoter (p16^{INK4A}-sgRNA-1 and -2), we detected a specific peak encompassing the *ARF* promoter and the identified distal repressive element, as well as the expected peak at the $p16^{INK4A}$ promoter (Fig. 4B). Comparing our Cas9 CUT&RUN data with the CTCF and H3K27ac Chromatin Immunoprecipitation Sequencing (ChIP-seq) data that demarcated compartment boundaries, the interaction between *ARF* and $p16^{INK4A}$ genes appears to be supported by a convergent looping model mediated by the canonical CTCF/Cohesin complex (43, 44). In summary, these data support the idea that $p16^{INK4A}$ and *ARF* physically crosstalk by chromatin looping, providing a proximity environment to regulate their respective transcription.

The *ARF*/$p16^{INK4A}$ Chromatin Interaction and Transcriptional Regulation Is Functionally Detected in Human Neuroblastoma Cells. We hypothesized that the same chromatin interaction pattern seen in human B-ALL SEM cells may exist in other cancer cell types that maintain low expression and an intact genomic sequence of $p16^{INK4A}$. To this end, we transduced lentiviral dCas9-KRAB with ARF-sgRNA-3 and -4 into a human neuroblastoma (NBL) cell line, SK-N-SH. ARF-sgRNA-4, but not sgRNA-3, could significantly up-regulate the expression of $p16^{INK4A}$ consistently at mRNA and protein levels (Fig. 5 A–C). Both sgRNAs conversely decreased *ARF* expression. During in vitro culture of targeted cells, we observed significant growth retardation using ARF-sgRNA-4, consistent with specific up-regulation of $p16^{INK4A}$ (Fig. 5 D and E). The 3C libraries were prepared from SK-N-SH dCas9-KRAB stable cells targeted with either
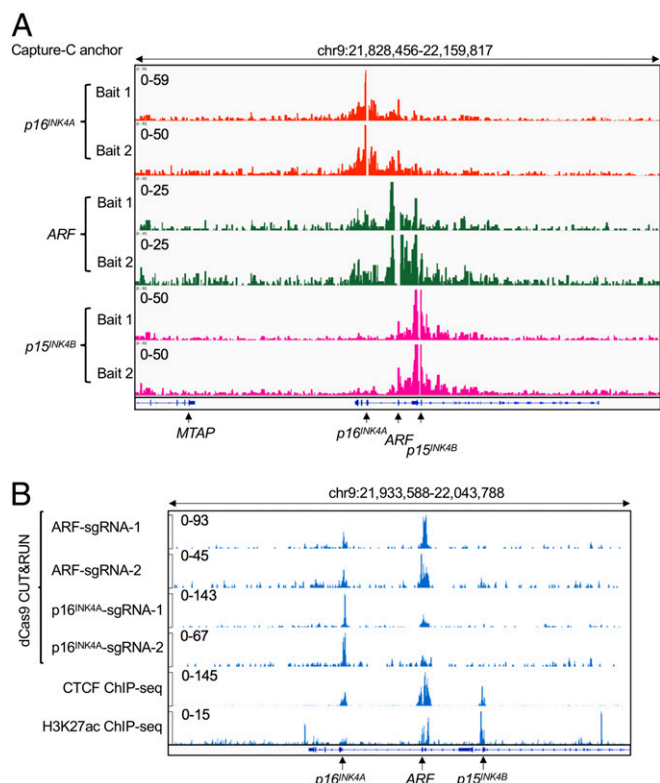
Fig. 4. Physical interactions between *ARF*, *p16^INK4A^*, and *p15^INK4B^* were detected by 3C. (*A*) Next-generation Capture-C was performed on parental human SEM cells for 2 replicates. Two specific anchor probes (Bait 1 and Bait 2) were designed to hybridize to the H3K27ac peaks that overlap each of the promoters of *p16^INK4A^*, *ARF*, and *p15^INK4B^* to capture chromatin interactions with the respective promoters within the *INK4/ARF* locus. (*B*) CUT&RUN was performed on *p16^mCherry/+;dCas9-KRAB^* cells infected individually with 2 sgRNAs targeting the *p16^INK4A^* repressive element adjacent to the *ARF* promoter and 2 sgRNAs targeting the *p16^INK4A^* promoter. A Cas9 antibody that recognizes dCas9 was used for a pull-down assay. ChIP-seq tracks of CTCF and H3K27ac were included to indicate the open chromatin status of the locus.

nontargeting-sgRNA (NT-sgRNA) or ARF-sgRNA-4. When Capture-C was performed using bait oligonucleotides against the *p16^INK4A^* promoter on the NT-sgRNA 3C library, the *p16^INK4A^* promoter was juxtaposed to both *ARF* and *p15^INK4B^*. However, the *ARF*/*p16^INK4A^* and *p16^INK4A^*/*p15^INK4B^* looping affinity was significantly reduced in Capture-C using *p16^INK4A^* promoter bait oligonucleotides on the ARF-sgRNA-4 3C library (Fig. 5 *F* and *G*).

Loss-of-Function CRISPR/Cas9 Screening of Human Transcription Factors in the *p16^INK4A^* Reporter Cell Line. We further undertook a comprehensive loss-of-function CRISPR-Cas9 screen targeting 1,639 human transcription factors in combination with the *p16^mCherry/+^* reporter system to identify putative regulatory effectors. Seven sgRNAs were designed for each transcription factor (TF), and an additional 100 nontargeting sgRNAs were included as negative controls (Fig. 6*A*). Similar to previous noncoding screening, about 1 million cells from the top 10% (mCherry^High^) and bottom 10% (mCherry^Low^) sorted populations were collected for deep sequencing to identify differentially represented sgRNAs.

Surprisingly, the most characterized looping factor, CTCF, was not enriched in the screen (Fig. 6*B*). Furthermore, we utilized a previously described auxin inducible degron system (45–47) to acutely deplete the CTCF protein in SEM cells (*SI Appendix*, Fig. S7 *A–D*) (33). Although the CUT&RUN using CTCF antibody for chromatin pull-down demonstrated loss of CTCF occupancy throughout the *INK4/ARF* locus (*SI Appendix*, Fig. S7*E*), perturbation of CTCF did not alter p16^INK4A^ expression changes at the mRNA or protein levels (*SI Appendix*, Fig. S6 *F* and *G*), suggesting that the *ARF*/*p16^INK4A^* interaction in SEM cells relies primarily on other looping factors.

The top-ranked candidate of positive regulators was Yin Yang 1 (YY1) (Fig. 6 *B* and *C*), which belongs to the GLI-Kruppel class of zinc-finger transcription factors and is ubiquitously expressed in most tissue and cell lines. YY1 plays a fundamental role in normal biologic processes such as embryogenesis, differentiation, replication, cellular proliferation, and cancer development (48, 49). Recently, YY1 was also reported to bind to active enhancers and promoter-adjacent elements and to form dimers that facilitate the interactions of these DNA elements (50–52). In the *p16^mCherry/+;dCas9-KRAB^* stable cell line, 2 sgRNAs (YY1-sgRNA-1 and -2) targeting the coding sequence of YY1 downregulated YY1 expression along with a reduction of reporter activity (Fig. 6 *E* and *F*). Although shown to act as a positive regulator of *p16^INK4A^* from the TF screen, YY1 was identified as a candidate transcription factor for the *ARF*/*p16^INK4A^* interaction due to a conserved YY1-binding motif in the previously identified 42-bp DNA segment within the *cis*-regulatory element (Fig. 6*G*). Additionally, YY1 occupancy at both *ARF* and *p16^INK4A^* promoters was confirmed in NT-sgRNA SEM^dCas9-KRAB^ cells by CUT&RUN assay. In ARF-sgRNA-4–targeted cells, YY1-binding affinity to *ARF*, but not to *p16^INK4A^*, was significantly disrupted (Fig. 6*H*). These paradoxical findings suggest that, while YY1 could facilitate the *ARF*/*p16^INK4A^* chromatin interaction that leads to *p16^INK4A^* repression, YY1's function across the *INK4/ARF* locus could be more complex due to genome-wide occupancy. Indeed, ChIP-seq data showed that YY1 occupancy extends across the *INK4/ARF* locus to include the TAD boundaries, the tumor suppressor genes, and the large superenhancer cluster (*SI Appendix*, Fig. S7*A*), underscoring that its activity could be widespread across the locus.

From the TF screen, we additionally identified the top 10 potential negative regulators repressing *p16^INK4A^* expression including CREB1, TFDP1, E2F2, TBP, ZNF217, THAP11, NKRF, C/EBPα, ZBTB14, and HMX3 (Fig. 6 *C* and *D*). C/EBPα has been recognized as an essential collaborator in Hoxa9/Meis1-mediated mouse leukemogenesis by directly repressing the *Cdkn2a/b* locus (53). Additionally, the p15^INK4B^ tumor suppressor has also been identified as a direct target of the ZNF217/CoREST transcriptional complex (54). To test if the putative negative regulator ZNF217 interacted with the locus, CUT&RUN using a specific antibody against ZNF217 was performed in SEM cells stably expressing dCas9-KRAB and either NT-sgRNA or ARF-sgRNA-4. ZNF217 occupancy on both the *p16^INK4A^* promoter and its distal repressive element in *ARF* was observed in NT-sgRNA SEM cells (Fig. 6*I*). However, in ARF-sgRNA-4–targeted cells, ZNF217-binding affinity to *ARF* and *p16^INK4A^*, but not other loci, was significantly disrupted (Fig. 6 *I* and *J*), demonstrating that a looped conformation was a prerequisite for ZNF217 binding and suggesting that ZNF217 may play an important role in *p16^INK4A^* repression defined by the long-distance chromatin interaction model. Although we specifically addressed ZNF217's interaction with *ARF*/*p16^INK4A^*, we anticipate that other negative regulators identified in the screen could behave similarly. Collectively, by presenting an unbiased, genome-scale loss-of-function TF screen, we identified plausible transcriptional regulators of *p16^INK4A^*.

Discussion

We identified a *cis*-element located in the 3′ region adjacent to the *ARF* promoter that represses *p16^INK4A^* expression via the formation of long-range chromosomal contacts. The identification of a *p16^INK4A^* distal repressive element located 3′ and adjacent to the ARF promoter is in accord with previous observations that p16^Ink4a^ expression was significantly up-regulated in *Arf*-null
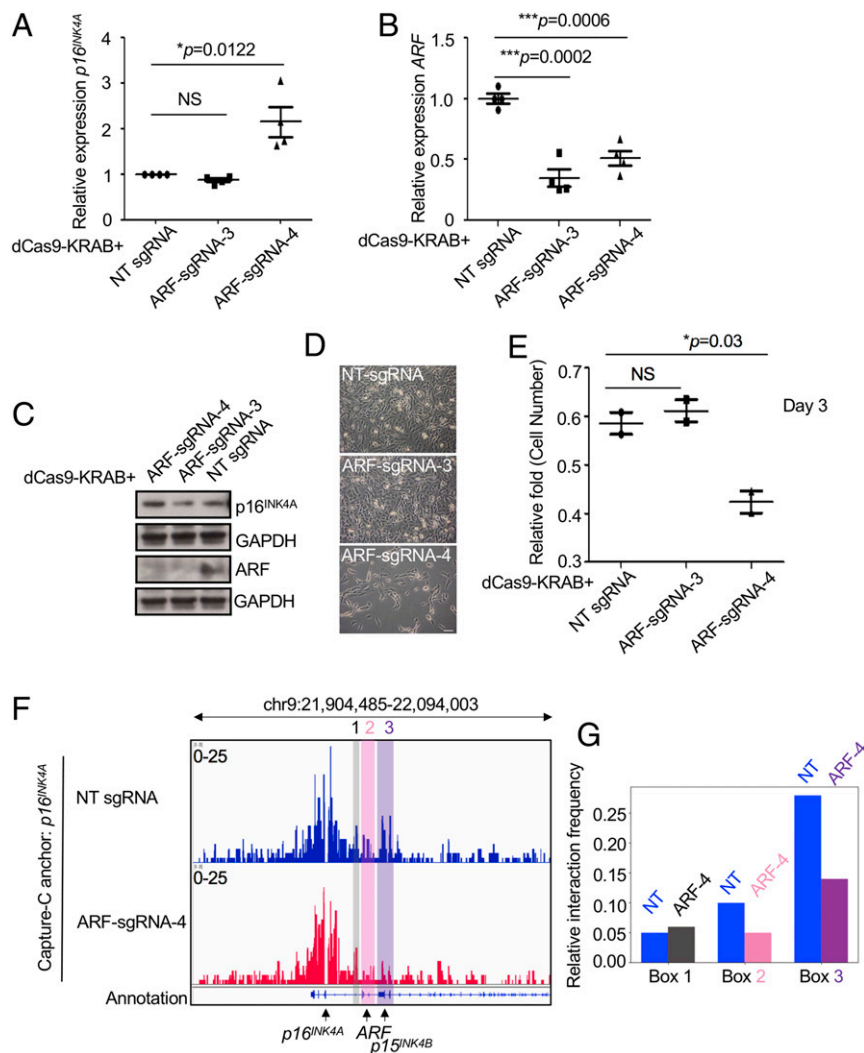
Fig. 5. The $ARF/p16^{INK4A}$ chromatin interaction and transcriptional regulation is functionally detected in NBL cells. (*A*) qRT-PCR analysis of $p16^{INK4A}$ in the human NBL cell line SK-*N*-SH infected with lentiviral dCas9-KRAB and ARF-sgRNAs-3 and -4. NT-sgRNA is a nontargeting sgRNA control. Four biological replicates were performed. The *P* value was calculated by a 2-tailed *t* test. (*B*) qRT-PCR analysis of *ARF* in the human NBL cell SK-*N*-SH infected with lentiviral dCas9-KRAB and ARF-sgRNAs-3 and -4. Four biological replicates were performed. The *P* value was calculated by a 2-tailed *t* test. (*C*) Western blotting analysis of ARF and $p16^{INK4A}$ in the human NBL cell line SK-*N*-SH infected with lentiviral dCas9-KRAB and ARF-sgRNA-3 and -4 compared to NT-infected controls. (*D*) Representative image of SK-*N*-SH cells stably expressing dCas9-KRAB and ARF-sgRNAs-3, -4, and NT-sgRNA at day 3. (*E*) Quantification of cell proliferation by cell number count. Two biological replicates were performed. The *P* value was calculated by a 2-tailed *t* test. (*F*) Next-generation Capture-C was performed on SK-*N*-SH cells stably expressing dCas9-KRAB and ARF-sgRNAs-3, -4, and NT-sgRNA. Anchor probes that hybridized to the $p16^{INK4A}$ promoter were utilized to capture chromatin interactions. Boxes 2 and 3 highlight *ARF* and $p15^{INK4B}$ promoters which were interacting with the indicated $p16^{INK4A}$ anchor regions. Box 1 indicates a negative control noncoding region. (*G*) Quantification of interaction frequency between the anchor regions to Boxes 1, 2, and 3. Signal value from the .bw file of Capture-C was normalized by probe signal for each experiment.

mouse embryo fibroblasts, as well as in pre-B lymphocytes and keratinocytes lacking exon 1β (55, 56).

In mammalian cells, each chromosome is hierarchically organized into hundreds of megabase-sized TADs (57). Promoter/enhancer contacts take place within the TAD scaffold, leading to regulated gene expression (58). Intra-TAD chromatin interactions can be facilitated by a pair of CTCF-binding sites engaged in contact with each other when they are in a convergent linear orientation (44, 59). Using a chromosome conformation capture-based PCR assay, Hirosue et al. (11) proposed that CTCF was crucial for higher-order chromatin organization within the INK4/ARF locus and demonstrated that depletion of CTCF disrupted chromatin interactions and reactivated locus transcription in human induced pluripotent stem cells. In our study, by a high-resolution Capture-C assay, we showed that ARF, $p16^{INK4A}$, and $p15^{INK4B}$ can make physical contacts with each other over long

distances. By analyzing publicly available CTCF ChIP-seq data, we found that CTCF showed strong binding affinity to all 3 tumor suppressor promoters at the INK4/ARF locus. However, the loss-of-function results from auxin-inducible degradation of CTCF and the unbiased TF screening did not support the hypothesis that CTCF drives transcriptional regulation within $p16^{INK4A}$ in SEM cells.

Disruption of the $ARF/p16^{INK4A}$ interaction abrogated occupancy of ZNF217 to both ARF and $p16^{INK4A}$, highlighting that ZNF217 binding is dependent on the $ARF/p16^{INK4A}$ looped chromatin conformation. We propose a 2-step model for chromatin looping regulation of $p16^{INK4A}$. First, chromatin looping factors (e.g., YY1 or others) bind to the $p16^{INK4A}$ distal regulatory element adjacent to the ARF promoter and $p16^{INK4A}$ simultaneously to facilitate their physical juxtaposition and functional chromatin interaction. Once both genes are in physical contact,
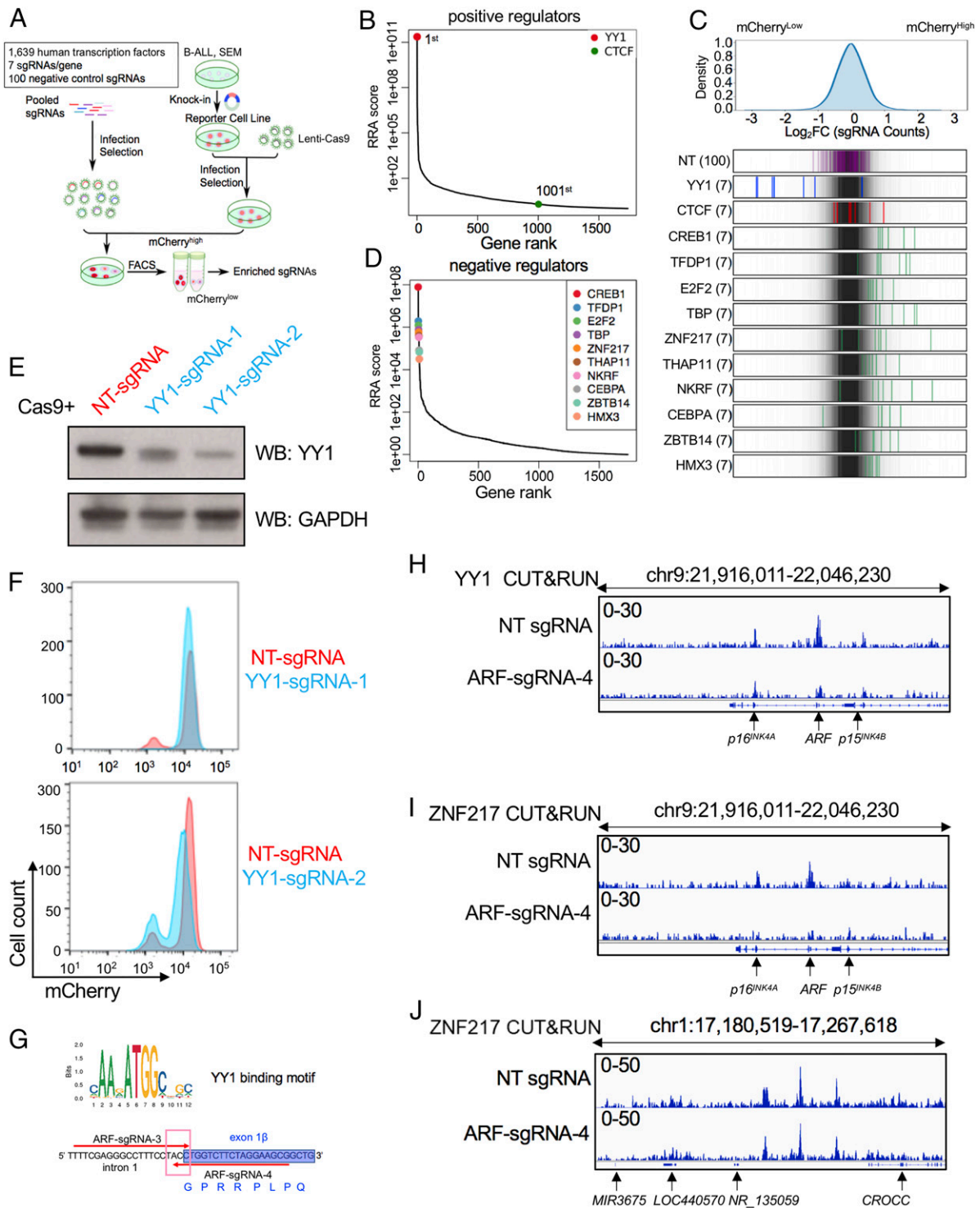
Fig. 6. Loss-of-function CRISPR screening of human transcriptional factors in the $p16^{INK4A}$ reporter cell line. (*A*) Schematic diagram of a working model of Cas9-mediated CRISPR screening targeting 1,639 human TFs. (*B*) Gene ranking of looping factors (YY1, first; CTCF, 1,001st) enriched from screening. The enrichment score of 7 sgRNAs against each TF was combined by MAGeCK algorithm. (*C, Top*) The overall distribution of all sgRNAs from the screening. (*C, Bottom*) The Log$_2$[Fold Change (top10/bottom10)] ratio for all sgRNAs targeting CTCF, YY1, and the top 10 negative regulators from *D* and NT sgRNAs were overlaid on a gray gradient depicting the overall distribution. NT: 100 gRNAs; TF: 7 sgRNAs/each. (*D*) Gene ranking of top 10 negative candidate regulators enriched from screening analysis by MAGeCK algorithm. (*E*) Immunoblotting of YY1 in $p16^{mCherry/+;Cas9}$ cells targeted individually with 2 sgRNAs against the coding sequence of human YY1. GAPDH was probed as a loading control. (*F*) The $p16^{mCherry/+;Cas9}$ cells were targeted with Cas9 and 2 sgRNAs identified from TF screening targeting the coding region of human YY1. Flow cytometry analysis of mCherry reporter activity was subsequently conducted in YY1-targeted cells compared with NT control. (*G*) YY1-binding motif prediction by JASPAR algorithm. (*H*) CUT&RUN of YY1 was conducted in $p16^{mCherry/+;dCas9-KRAB}$ cells infected with ARF-sgRNA-4 and NT-sgRNA for 2 replicates. Tracks were shown at the viewpoint of the *INK4/ARF* locus. (*I*) CUT&RUN of ZNF217 was conducted in $p16^{mCherry/+;dCas9-KRAB}$ cells infected with ARF-sgRNA-4 and NT-sgRNA. Tracks were shown at the viewpoint of the *INK4/ARF* locus. (*J*) CUT&RUN of ZNF217 was conducted in $p16^{mCherry/+;dCas9-KRAB}$ cells infected with ARF-sgRNA-4 and NT-sgRNA. Tracks of ZNF217 were shown for viewpoint at a randomly chosen locus.

repressive effectors such as ZNF217 and/or other transcription factors are recruited to the target sequence to enable $p16^{INK4A}$ transcriptional repression. We further suspect that additional candidate transcription factors identified from the transcription factor CRISPR/Cas9 screen might contribute as well, thereby providing a more comprehensive understanding about how the locus is regulated in human cells.

Materials and Methods

General Methods. All primers, plasmids, and reagents used in this study are cataloged in Dataset S1. Routine methods regarding cell culture, plasmid construction, transfection, electroporation, flow cytometry, immunoblotting, qRT-PCR, FISH, Capture-C, CUT&RUN, and statistics analysis are described in detail in *SI Appendix*.

Establishment of a $p16^{INK4A-P2A-mCherry}$ Reporter Cell Line. SEM were electroporated by using the Nucleofector-2b device (Lonza) with the V-kit and program X-001. For $p16^{INK4A-P2A-mCherry}$ knock-in delivery, 2.5 μg of the donor plasmid and 2.5 μg of the CRISPR/Cas9-p16^{INK4A}-C terminus-sgRNA all-in-one plasmid were used for 5 million SEM cells. Twenty-four hours after transfection, cells were sorted for the CRISPR/Cas9-p16^{INK4A}-C terminus-sgRNA vector GFP fluorescent marker to enrich the transfected cell population. After sorted cells recovered in culture for up to 3 wk, a second sort was performed to select cells for successful knock-in by sorting for cells expressing the mCherry fluorescent marker. Two weeks later, a third sort was repeated, and single-cell–derived colonies were picked up and expanded for knock-in characterization.

CRISPR Library Construction and Screening. A set of 2,029 sgRNA oligos that target H3K27ac and ATAC-seq positive peaks defined in the TAD containing *INK4/ARF* in IMR90, HCT116, and SEM cells as well as an additional 20 non-targeting control sgRNAs with no detectable match to the human genome were designed for array-based oligonucleotide synthesis (CustomArray). To construct a sgRNA pooled library targeting human TFs, 7 sgRNAs were designed against each of the 1,639 human TFs. For each library, the synthesized oligo pool was amplified by PCR and cloned into LentiGuide-Puro backbone (#52963) by in-fusion assembly (Clontech). The sgRNA sequences were recovered by genomic PCR and Deep Sequencing using MiSeq for single-end 150-bp read length (Illumina). The primer sequences used for cloning and sequencing are listed in Dataset S1. The sgRNA sequences related to CRISPR screening are described in Datasets S2 and S3.

Capture-C. Capture-C assay was conducted as described by Davies et al. (41) and Hyle et al. (33). Detailed protocol was provided in *SI Appendix*.

1. C. J. Sherr, The *INK4a/ARF* network in tumour suppression. *Nat. Rev. Mol. Cell Biol.* **2**, 731–737 (2001).
2. C. J. Sherr, Ink4-Arf locus in cancer and aging. *Wiley Interdiscip. Rev. Dev. Biol.* **1**, 731–741 (2012).
3. C. J. Sherr, D. Beach, G. I. Shapiro, Targeting CDK4 and CDK6: From discovery to therapy. *Cancer Discov.* **6**, 353–367 (2016).
4. M. Serrano et al., Role of the *INK4a* locus in tumor suppression and cell mortality. *Cell* **85**, 27–37 (1996).
5. T. Kamijo et al., Tumor suppression at the mouse *INK4a* locus mediated by the alternative reading frame product p19^{ARF}. *Cell* **91**, 649–659 (1997).
6. C. Kandoth et al., Mutational landscape and significance across 12 major cancer types. *Nature* **502**, 333–339 (2013).
7. A. V. Molofsky et al., Increasing p16^{INK4a} expression decreases forebrain progenitors and neurogenesis during ageing. *Nature* **443**, 448–452 (2006).
8. V. Janzen et al., Stem-cell ageing modified by the cyclin-dependent kinase inhibitor p16^{INK4a}. *Nature* **443**, 421–426 (2006).
9. R. A. J. Signer, E. Montecino-Rodriguez, O. N. Witte, K. Dorshkind, Aging and cancer resistance in lymphoid progenitors are linked processes conferred by p16^{Ink4a} and Arf. *Genes Dev.* **22**, 3115–3120 (2008).
10. J. Krishnamurthy et al., p16^{INK4a} induces an age-dependent decline in islet regenerative potential. *Nature* **443**, 453–457 (2006).
11. A. Hirosue et al., Quantitative assessment of higher-order chromatin structure of the *INK4/ARF* locus in human senescent cells. *Aging Cell* **11**, 553–556 (2012).
12. P. Rajendran et al., Nrf2 status affects tumor growth, *HDAC3* gene promoter associations, and the response to sulforaphane in the colon. *Clin. Epigenetics* **7**, 102 (2015).
13. R. Zhao, B. Y. Choi, M.-H. Lee, A. M. Bode, Z. Dong, Implications of genetic and epigenetic alterations of *CDKN2A* (p16^{INK4a}) in cancer. *EBioMedicine* **8**, 30–39 (2016).
14. D. J. Baker et al., Clearance of p16^{Ink4a}-positive senescent cells delays ageing-associated disorders. *Nature* **479**, 232–236 (2011).
15. B. G. Childs, M. Durik, D. J. Baker, J. M. van Deursen, Cellular senescence in aging and age-related disease: From mechanisms to therapy. *Nat. Med.* **21**, 1424–1435 (2015).
16. E. Pasmant, A. Sabbagh, M. Vidaud, I. Bièche, ANRIL, a long, noncoding RNA, is an unexpected major hotspot in GWAS. *FASEB J.* **25**, 444–448 (2011).
17. W. R. Jeck, A. P. Siebold, N. E. Sharpless, Review: A meta-analysis of GWAS and age-associated diseases. *Aging Cell* **11**, 727–731 (2012).
18. T. S. Klann et al., CRISPR-Cas9 epigenome editing enables high-throughput screening for functional regulatory elements in the human genome. *Nat. Biotechnol.* **35**, 561–568 (2017).
19. M. G. Callow et al., CRISPR whole-genome screening identifies new necroptosis regulators and RIPK1 alternative splicing. *Cell Death Dis.* **9**, 261 (2018).
20. S. M. Sidik, D. Huet, S. Lourido, CRISPR-Cas9-based genome-wide screening of Toxoplasma gondii. *Nat. Protoc.* **13**, 307–323 (2018).
21. J. Du et al., A CRISPR/Cas9-based screening for non-homologous end joining inhibitors reveals ouabain and penfluridol as radiosensitizers. *Mol. Cancer Ther.* **17**, 419–431 (2018).
22. J. D. Grevet et al., Domain-focused CRISPR screen identifies HRI as a fetal hemoglobin regulator in human erythroid cells. *Science* **361**, 285–290 (2018).
23. T. Gonatopoulos-Pournatzis et al., Genome-wide CRISPR-Cas9 interrogation of splicing networks reveals a mechanism for recognition of autism-misregulated neuronal microexons. *Mol. Cell* **72**, 510–524.e12 (2018).
24. J. T. Irelan et al., A functional screen for regulators of CKDN2A reveals MEOX2 as a transcriptional activator of INK4a. *PLoS One* **4**, e5067 (2009).
25. K. Yamakoshi et al., Real-time in vivo imaging of p16^{Ink4a} reveals cross talk with p53. *J. Cell Biol.* **186**, 393–407 (2009).
26. M. Demaria et al., An essential role for senescent cells in optimal wound healing through secretion of PDGF-AA. *Dev. Cell* **31**, 722–733 (2014).
27. J.-Y. Liu et al., Cells exhibiting strong p16^{INK4a} promoter activation in vivo display features of senescence. *Proc. Natl. Acad. Sci. U.S.A.* **116**, 2603–2611 (2019).
28. C. E. Burd et al., Monitoring tumorigenesis and senescence in vivo with a p16$^{(INK4a)}$-luciferase model. *Cell* **152**, 340–351 (2013).
29. J. A. Sorrentino et al., p16^{INK4a} reporter mice reveal age-promoting effects of environmental toxicants. *J. Clin. Invest.* **124**, 169–173 (2014).
30. J. H. Kim et al., High cleavage efficiency of a 2A peptide derived from porcine teschovirus-1 in human cell lines, zebrafish and mice. *PLoS One* **6**, e18556 (2011).
31. J. P. Zhang et al., Efficient precise knockin with a double cut HDR donor after CRISPR/Cas9-mediated double-stranded DNA cleavage. *Genome Biol.* **18**, 35 (2017).
32. X. Yao et al., Homology-mediated end joining-based targeted integration using CRISPR/Cas9. *Cell Res.* **27**, 801–814 (2017).
33. J. Hyle et al., Acute depletion of CTCF directly affects *MYC* regulation through loss of enhancer-promoter looping. *Nucleic Acids Res.* **47**, 6699–6713 (2019).
34. L. A. Gilbert et al., CRISPR-mediated modular RNA-guided regulation of transcription in eukaryotes. *Cell* **154**, 442–451 (2013).
35. M. Demaria et al., Cellular senescence promotes adverse effects of chemotherapy and cancer relapse. *Cancer Discov.* **7**, 165–176 (2017).
36. J. D. Buenrostro, P. G. Giresi, L. C. Zaba, H. Y. Chang, W. J. Greenleaf, Transposition of native chromatin for fast and sensitive epigenomic profiling of open chromatin, DNA-binding proteins and nucleosome position. *Nat. Methods* **10**, 1213–1218 (2013).
37. M. P. Creyghton et al., Histone H3K27ac separates active from poised enhancers and predicts developmental state. *Proc. Natl. Acad. Sci. U.S.A.* **107**, 21931–21936 (2010).
38. K. D. Robertson, P. A. Jones, The human *ARF* cell cycle regulatory gene promoter is a CpG island which can be silenced by DNA methylation and down-regulated by wild-type p53. *Mol. Cell. Biol.* **18**, 6457–6473 (1998).
39. M. I. Love, W. Huber, S. Anders, Moderated estimation of fold change and dispersion for RNA-seq data with DESeq2. *Genome Biol.* **15**, 550 (2014).
40. J. R. Hughes et al., Analysis of hundreds of cis-regulatory landscapes at high resolution in a single, high-throughput experiment. *Nat. Genet.* **46**, 205–212 (2014).
41. J. O. J. Davies et al., Multiplexed analysis of chromosome conformation at vastly improved sensitivity. *Nat. Methods* **13**, 74–80 (2016).
42. P. J. Skene, S. Henikoff, An efficient targeted nuclease strategy for high-resolution mapping of DNA binding sites. *eLife* **6**, e21856 (2017).
43. E. de Wit et al., CTCF binding polarity determines chromatin looping. *Mol. Cell* **60**, 676–684 (2015).
44. S. S. Rao et al., A 3D map of the human genome at kilobase resolution reveals principles of chromatin looping. *Cell* **159**, 1665–1680 (2014).
45. K. Nishimura, M. T. Kanemaki, Rapid depletion of budding yeast proteins via the fusion of an auxin-inducible degron (AID). *Curr. Protoc. Cell Biol.* **64**, 20.9.1–20.9.16 (2014).
46. T. Natsume, T. Kiyomitsu, Y. Saga, M. T. Kanemaki, Rapid protein depletion in human cells by auxin-inducible degron tagging with short homology donors. *Cell Rep.* **15**, 210–218 (2016).

47. E. P. Nora et al., Targeted degradation of CTCF decouples local insulation of chromosome domains from genomic compartmentalization. *Cell* **169**, 930–944.e22 (2017).

48. W. Wang, D. Li, G. Sui, YY1 is an inducer of cancer metastasis. *Crit. Rev. Oncog.* **22**, 1–11 (2017).

49. F. Chen, H. Sun, Y. Zhao, H. Wang, YY1 in cell differentiation and tissue development. *Crit. Rev. Oncog.* **22**, 131–141 (2017).

50. M. Makhlouf et al., A prominent and conserved role for YY1 in Xist transcriptional activation. *Nat. Commun.* **5**, 4878 (2014).

51. J. A. Beagan et al., YY1 and CTCF orchestrate a 3D chromatin looping switch during early neural lineage commitment. *Genome Res.* **27**, 1139–1152 (2017).

52. A. S. Weintraub et al., YY1 is a structural regulator of enhancer-promoter loops. *Cell* **171**, 1573–1588.e28 (2017).

53. C. Collins et al., C/EBPα is an essential collaborator in Hoxa9/Meis1-mediated leukemogenesis. *Proc. Natl. Acad. Sci. U.S.A.* **111**, 9899–9904 (2014).

54. G. Thillainadesan et al., TGF-β-dependent active demethylation and expression of the p15ink4b tumor suppressor are impaired by the ZNF217/CoREST complex. *Mol. Cell* **46**, 636–649 (2012).

55. A. W. Lin, S. W. Lowe, Oncogenic ras activates the ARF-p53 pathway to suppress epithelial cell transformation. *Proc. Natl. Acad. Sci. U.S.A.* **98**, 5025–5030 (2001).

56. D. H. Randle, F. Zindy, C. J. Sherr, M. F. Roussel, Differential effects of p19(Arf) and p16(Ink4a) loss on senescence of murine bone marrow-derived preB cells and macrophages. *Proc. Natl. Acad. Sci. U.S.A.* **98**, 9654–9659 (2001).

57. J. R. Dixon et al., Topological domains in mammalian genomes identified by analysis of chromatin interactions. *Nature* **485**, 376–380 (2012).

58. A. Pombo, N. Dillon, Three-dimensional genome architecture: Players and mechanisms. *Nat. Rev. Mol. Cell Biol.* **16**, 245–257 (2015).

59. M. Vietri Rudan et al., Comparative Hi-C reveals that CTCF underlies evolution of chromosomal domain architecture. *Cell Rep.* **10**, 1297–1309 (2015).